EMBRAER ICING CONSULTATION

ESI Project: 48658C

4775 Centennial Boulevard, Suite 106
Colorado Springs, CO 80919

EMBRAER ICING CONSULTATION

ESI Project: 48658C

Report Prepared for:

Embraer S.A.
Av. Brigadeiro Faria Lima, 2.170
12227-901 - San Jose dos Campos - SP
Brazil

Submitted by:

Steven L. Morris, Ph.D., P.E.
Senior Managing Consultant & Manager of Colorado Operations
Colorado P.E. | Expires: 10/31/2016

04/08/2016
Date

Technical Review by:

Robert C. Winn, Ph.D., P.E.
Chairman of the Board, Principal & Director - Aviation
Colorado P.E. | Expires: 10/31/2016

04/08/2016
Date

INTRODUCTION

Engineering Systems Inc. (ESI) was retained by Embraer S. A. to perform an analysis of the ice accretion on the wing and horizontal stabilizer of an Embraer EMB-500 Phenom 100 Jet. The flight and atmospheric conditions analyzed were those that existed at the time of the accident of Embraer EMB-500, N100EQ, which occurred on December 8, 2014 near Gaithersburg, Maryland. The icing analysis was performed using environmental conditions provided by Dr. Wayne Sand, flight conditions determined from the on-board Cockpit Voice and Data Recorder (CVDR) and derived from recorded Air Traffic Control radar data, and wing and horizontal stabilizer geometry supplied by Embraer. It was assumed and confirmed by the CVDR that the de-icing boots were not operated throughout the icing conditions analyzed. The study was performed using the two-dimensional NASA code, LEWICE 3.2.2, developed by the NASA Glenn Research Center (GRC), to analyze the ice accretion on the exposed surfaces of an air vehicle and/or wing sections. Water droplet trajectories and ice accretions were computed around 2D models of cross sections at selected locations on the aircraft wing and horizontal stabilizer.

AIRCRAFT VEHICLE MODEL ANALYZED

To determine the ice accretion encountered during the accident scenario three two-dimensional airfoil cross sections along the wing span and three two-dimensional airfoil cross sections along the horizontal tail span were analyzed using LEWICE 3.2.2 at the appropriate flight and meteorological conditions. The geometric data for each of the six cross sections were provided by Embraer. Figure 1 provides a three-dimensional drawing of half of the aircraft with the three wing cross sections and the three horizontal tail cross sections identified in red.[1] Figure 2 provides a view of the cross sections only.

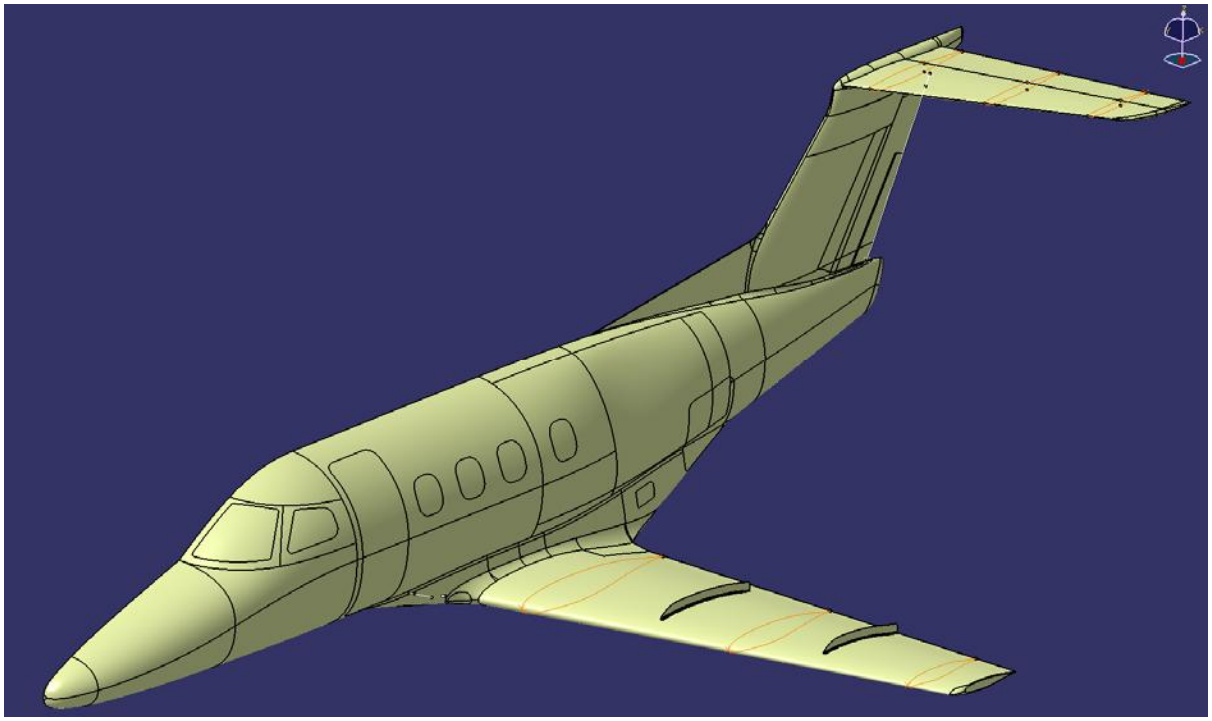

Figure 1. EMB-500 Phenom 100 Jet with Wing and Horizontal Tail Locations Analyzed[1]

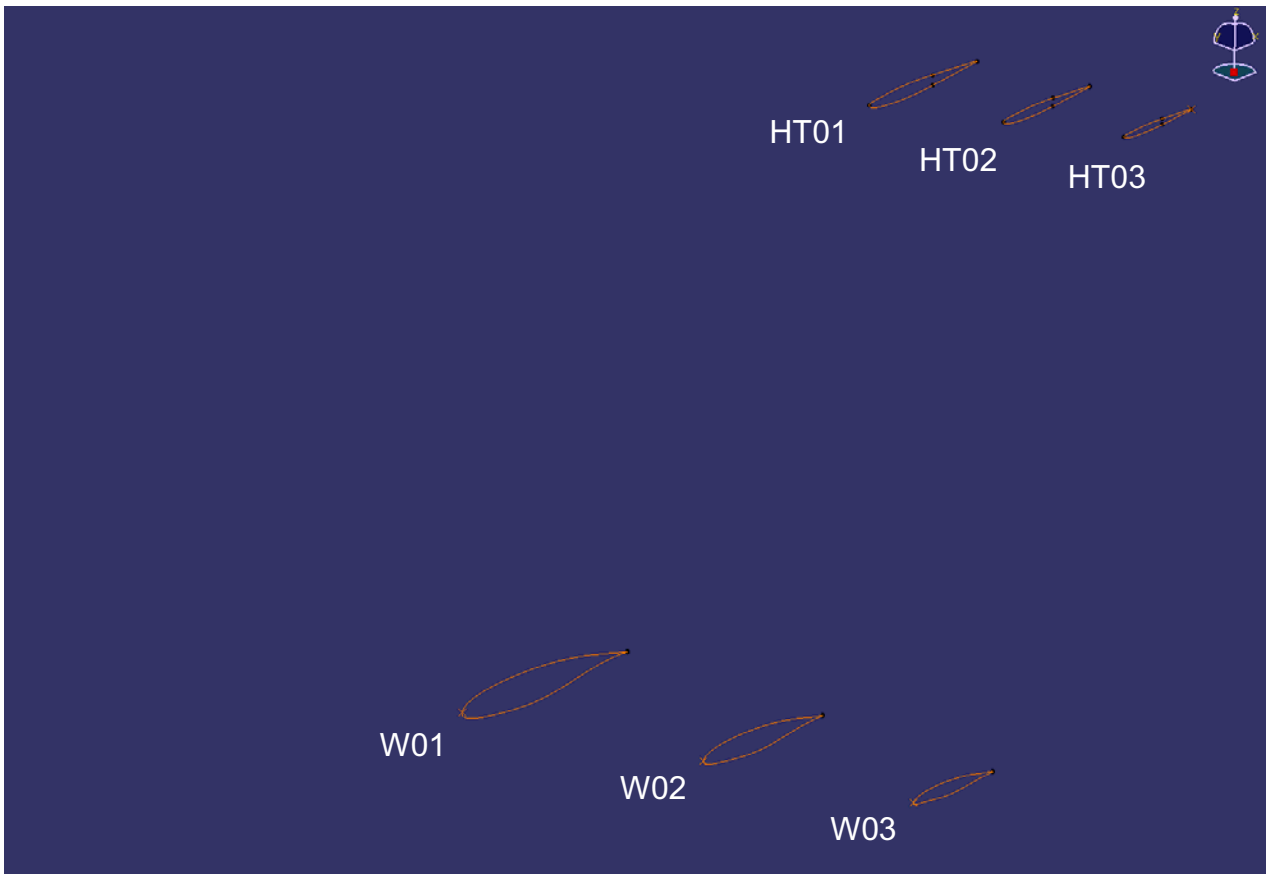

Figure 2. View of Wing and Horizontal Tail Cross Sections Analyzed[1]

The wing station locations and chord lengths of each of the six cross sections analyzed are shown below in Table 1. Note that W01, W02, and W03 correspond to inboard, mid, and outboard spanwise locations along the wing, respectively. Similarly, HT01, HT02, and HT03 correspond to an inboard, mid, and outboard spanwise location along the horizontal tail, respectively.

Cut Number	Wing Station inches	Chord inches
W01	51.181	76.529
W02	141.732	55.161
W03	220.472	36.597
HT01	11.811	49.787
HT02	51.181	39.901
HT03	86.614	31.003

Table 1: Wing Stations and Chords

LEWICE 3.2.2

The 2D computer software code, LEWICE 3.2.2, developed by NASA GRC was used in this study to analyze the ice accretion on the wing and horizontal tail cross sections. The software contains an analytical ice accretion model that evaluates the thermodynamics of the freezing process that occurs when supercooled droplets impinge on a body.[2] The flight parameters of airspeed and angle of attack and the meteorological conditions of temperature, pressure, liquid water content (LWC), droplet diameter, and relative humidity are specified and used to determine the amount and shape of the ice accretion.

The software consists of four major modules. They are 1) the flow field calculation using the Douglas Hess-Smith 2-D panel code (S24Y), 2) the particle trajectory and impingement calculation, 3) the thermodynamic and ice growth calculation, and 4) the modification of the current geometry by adding the ice growth to it. LEWICE applies a time-stepping procedure to "grow" the ice accretion. Initially, the flow field and droplet impingement characteristics are determined for the clean geometry. The ice growth rate on each segment defining the surface is then determined by applying the thermodynamic model. When a time increment is specified, this growth rate can be used to determine an ice thickness for that increment and the body coordinates are adjusted to account for the accreted ice. This procedure is repeated, beginning with the calculation of the flow field about the iced geometry, and continued until the desired icing time has been reached. The calculated results from LEWICE have been compared to experimental ice accretion shapes obtained both in flight and in the Icing Research Tunnel at NASA GRC in order to evaluate, improve, and validate the code.[3]

The LEWICE 3.2.2 analysis was accomplished using the computer program LEWINT[4] developed by the American Kestrel Company, LLC. The LEWINT program integrates the NASA ice accretion code, LEWICE 3.2.2, with a user's interface, icing analysis tools, and an automated plotting routine. American Kestrel distributes LEWINT under license with the NASA GRC.

LEWICE 3.2.2 TEST CONDITIONS

The ice accretion study was performed on each of the 2D cross sections during the time period that the aircraft was in meteorological conditions conducive to aircraft icing. The meteorological conditions that existed during the time of the accident flight of N100EQ were determined and supplied for this analysis by Dr. Wayne Sand and are provided in Table 2 below. These data consist of altitude above mean sea level (MSL), wind speed and direction, temperature, and liquid water content (LWC) and droplet diameter where appropriate. Table 2 shows that the icing level extends from approximately 2,400 feet MSL to 5,200 feet MSL (highlighted in the table). Below 2,400 feet MSL and above 5,200 feet MSL the aircraft is not operating in icing conditions and ice will not accrete on the aircraft.

Altitude Feet, MSL	Wind Direction degrees	Wind Speed knots	Temperature Degrees C	Liquid Water Content, g/m^3	Droplet Diameter, microns
279	40	7	-1.0		
400	42	8	-1.1		
600	45	9	-1.3		
800	47	10	-1.5		
1000	55	11	-1.9		

1200	62	12	-2.4		
1400	70	14	-2.8		
1600	77	15	-3.3		
1800	85	16	-3.8		
2000	92	17	-4.2		
2200	97	19	-4.0		
2400	102	20	-3.9	0.02	10
2600	107	22	-3.9	0.04	10
2800	112	23	-3.9	0.06	10
3000	115	23	-4.1	0.08	15
3200	116	21	-4.3	0.10	15
3400	118	19	-4.3	0.12	15
3600	119	17	-4.0	0.15	20
3800	121	15	-4.1	0.18	20
4000	122	14	-4.2	0.21	20
4200	121	14	-4.3	0.24	25
4400	120	14	-4.4	0.25	25
4600	120	14	-4.5	0.26	25
4800	119	14	-4.6	0.27	25
5000	118	14	-4.7	0.28	25
5200	119	14	-3.4	0.12	25
5400	122	13	-2.6		
5600	124	13	-1.8		
5800	126	12	-1.0		
6000	128	11	-0.9		
6200	129	12	-1.1		
6400	130	12	-1.3		
6600	130	13	-1.6		
6800	131	13	-1.9		
7000	132	14	-1.9		
7200	140	14	-1.5		
7400	148	14	-1.2		
7600	156	14	-0.9		
7800	164	14	-0.6		
8000	172	14	-0.2		
8200	173	13	0.1		
8400	174	13	0.4		
8600	176	12	0.4		
8800	177	12	0.1		

9000	178	11	-0.2		
9200	182	10	-0.6		
9400	187	9	-0.9		
9600	191	9	-1.3		
9800	195	8	-1.6		
10000	199	7	-2.0		
10200	203	6	-2.3		
10400	203	7	-2.8		
10600	204	8	-3.2		
10800	204	9	-3.6		
11000	204	10	-4.1		
11200	203	11	-4.5		
11400	202	11	-5.0		
11600	201	12	-5.4		
11800	200	13	-5.8		
12000	199	14	-6.3		
12200	198	15	-6.7		
12400	197	16	-7.1		
12600	197	17	-7.5		
12800	196	18	-7.8		
13000	195	19	-8.2		
13200	196	19	-8.5		
13400	197	18	-8.9		
13600	199	18	-9.3		
13800	200	18	-9.6		
14000	201	18	-10.0		
14200	203	18	-10.3		
14400	204	19	-10.7		
14600	206	19	-11.1		
14800	207	20	-11.6		
15000	209	20	-12.0		
15200	209	20	-12.5		
15400	209	20	-12.9		
15600	208	21	-13.4		
15800	208	21	-13.8		
16000	208	21	-14.3		
16200	208	22	-14.7		
16400	209	23	-15.1		
16600	209	23	-15.5		

16800	210	24	-16.0		
17000	210	25	-16.4		
17200	210	26	-16.8		
17400	210	26	-17.3		
17600	210	27	-17.7		
17800	210	27	-18.1		
18000	210	28	-18.6		
18200	210	29	-19.0		
18400	211	29	-19.5		
18600	211	30	-20.1		
18800	211	30	-20.6		
19000	210	30	-21.2		
19200	209	30	-21.7		
19400	209	30	-22.3		
19600	208	31	-22.8		
19800	208	31	-23.4		
20000	207	31	-23.9		
20200	208	32	-24.5		
20400	209	32	-25.0		
20600	210	33	-25.5		
20800	211	34	-26.1		
21000	212	34	-26.6		
21200	214	35	-27.1		
21400	215	35	-27.7		
21600	217	35	-28.2		
21800	218	36	-28.7		
22000	220	36	-29.3		
22200	221	36	-29.6		
22400	223	37	-30.0		
22600	225	37	-30.4		
22800	226	37	-30.8		
23000	228	37	-31.2		

Table 2. Summary of Meteorological Conditions Provided by Dr. Wayne Sand[5]

In addition to the meteorological conditions, the aircraft's true airspeed and angle of attack are important parameters in calculating the ice accretion, if any, on the aircraft. The flight conditions were initially determined from a flight path reconstruction using the recorded radar data. The wind and temperature data were used to determine the true and equivalent airspeeds. These conditions were later refined using parameters recorded by the CVDR. Since the airspeed, angle of attack, and meteorological conditions

vary throughout the flight, the flight within the icing environment was divided into six phases using the average conditions for each individual phase as inputs to the LEWICE code. This provides a more accurate calculation of the ice accretion than using a single average value for each of the parameters over the entire period the aircraft was in the icing environment. The six flight phases are provided in Table 3.

Phase	Altitude feet, msl	LEWICE Altitude feet	True Airspeed knots	Body Angle of Attack degrees	Temperature degrees C	Liquid Water Content g/m^3	Drop Diameter microns	Time seconds
I	5,200 to 5,000	5,100	260	0.54	-4.1	0.2	25	14
II	5,000	5,000	201	2.17	-4.7	0.28	25	275
IIIA	5,000 to 4,000	4,500	184	2.69	-4.5	0.25	24	91
IIIB	4,000 to 3,000	3,500	196	1.87	-4.2	0.14	18	79
IV	3,000	3,000	161	3.96	-4.1	0.08	15	390
V	3,000 to 2,400	2,700	136	4.47	-4.0	0.05	12	58

Table 3. Six Phases of Flight in Icing Conditions Used in LEWICE

The values shown in Table 3 are used as inputs to LEWICE and are average values for that phase of flight. The table shows the time in icing conditions for each phase of flight. Overall, the aircraft was in an environment conducive to icing for a total of approximately 907 seconds or 15 minutes and 7 seconds as it descended from 5,200 feet to 2,400 feet. The angle of attack values provided in Table 3 are with respect to the body axis of the aircraft. Therefore, the incidences of the wing and horizontal tail with respect to the body axis at each cross section location are needed by LEWICE to determine the geometric angle of attack and accurately predict the ice accretion. These values were provided by Embraer and are shown in Table 4. The differences in the wing incidences with respect to the aircraft body axis are a result of wing twist. The downwash produced by the wing will alter the effective angle of attack of the wing and horizontal tail but because of the relatively low angle of attack will have a minimal impact on the location and amount of the ice formation and was not used in the LEWICE analysis.

Cut Number	Wing Station inches	Incidence degrees
W01	51.1811	1.27
W02	141.7323	0.80
W03	220.4724	0.04
HT01	11.8110	-0.41
HT02	51.1811	-0.43
HT03	86.6142	-0.46

Table 4: Wing Stations and Incidence Angles

LEWICE 3.2.2 ANALYSIS METHODOLOGY

As discussed earlier, the analysis was performed using LEWINT, which is a program that provides a user-friendly interface for the NASA ice accretion code, LEWICE 3.2.2.

The methodology used began by inputting the Phase I test conditions into LEWINT (LEWICE 3.2.2) for a given wing or horizontal tail airfoil section. The code produces a number of output files to include the amount of ice accretion and a new cross section consisting of the original airfoil plus any accreted ice. The new cross section becomes the input for next LEWICE run using the Phase II input conditions. The output of that LEWICE run then becomes the input cross section to the Phase IIIA test conditions. This process is repeated until LEWICE has been completed for all six phases of flight resulting in a final cross section shape representing the original airfoil and all of the accumulated ice. The thickness of the ice as a function of the distance back along surface of the original airfoil, s, is computed by comparing the final iced airfoil cross section with the original airfoil cross section.

LEWICE 3.2.2 ANALYSIS RESULTS

The following summarizes the findings from the LEWICE analyses for each of the three wing cross sections and each of the three horizontal tail cross sections for the Phenom 100. The results shown provide the ice shape superimposed on the airfoil shape and the ice thickness as function of distance along the top and bottom surfaces of the airfoil for the entire 15-plus minutes of flight in the icing environment. Data are available for the ice shapes after each of the other five intermediate phases but are not included in this report.

Figure 3 provides a sample airfoil depicting the definition of the positive and negative distances "s" along the airfoil surface. The value of "s" is zero at the leading edge of the airfoil. The value of "s" in inches is the horizontal axis of the ice thickness plots that are presented in this report. Note that the leading edge does not necessarily correspond to the X–coordinate equal zero, Y-coordinate equal zero, (i.e., 0, 0), locations in the airfoil cross sections. Therefore, s equal to 0 does not necessarily correspond to X equal to 0, as X may be a very small negative number and Y may be positive or negative at the leading edge.

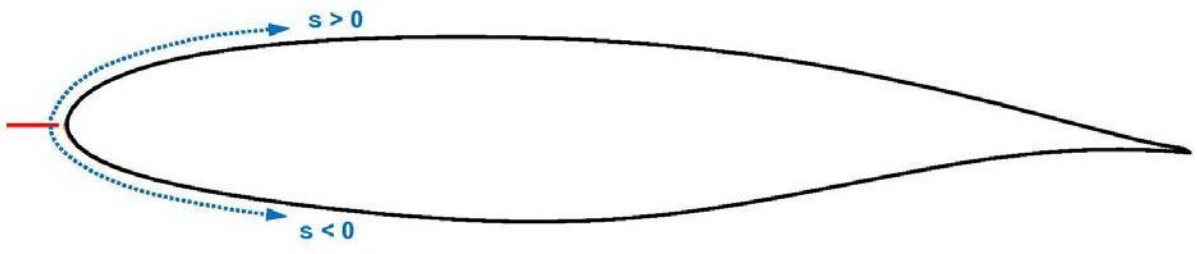

Figure 3. Definition of Positive and Negative Values of Distance Along Airfoil Surface, s

Wing Cross Section W01 (Inboard Wing Section) Results

The forward part of the wing cross section and the ice shape at location W01 is shown in Figure 4. This shows the ice that has been accreted during the 15-plus minute icing environment. A closer view of the leading edge of the airfoil in Figure 5 better reveals the ice accretion. Note that the ice does not accrete very far aft on the upper surface which would be well within the coverage of the de-icing boots. The ice shape also conforms with the shape of the airfoil. The implications of the formation of ice on the airfoil will be discussed later in the report.

The calculated ice thickness as a function of distance along the airfoil, s, is shown in Figure 6. The locations in the plot on the lower surface that go to zero between the none-zero ice thickness values do not show up in Figure 4 and are artifacts of the ice thickness calculation and should be ignored. This effect has been seen on thicker airfoils with relatively thin ice accretions. The maximum ice thickness is approximately 0.11 inches and occurs very near the leading edge of the airfoil and does not extend very far aft, well within the coverage of the pneumatic de-icing boots.

Wing Cross Section W02 (Mid-Span Wing Section) Results

The forward part of the wing cross section and ice shape at a mid-span location, W02, is shown below in Figure 7. Figure 8 provides a closer view of the leading edge of the airfoil and provides a better view of the ice that has accreted during the 15-plus minutes of exposure.

The calculated ice thickness as a function of distance along the airfoil, s, is shown in Figure 9. At this wing station the maximum ice thickness is slightly greater than 0.15 inches and occurs very near the leading edge of the airfoil. The ice at this location is thicker than at the inboard section, W01. This is expected since the airfoil cross section is smaller and thinner and, therefore, a more efficient ice collector. As with the ice shape at wing station W01 the ice does not accrete very far aft on the upper surface and would be well within the coverage of the de-icing boots.

Wing Cross Section W03 (Outboard Wing Section) Results

The wing cross section and ice shape at an outboard location, W03, is shown in Figure 10. Figure 11 provides a closer view of the forward portion of the airfoil and provides the shape of the ice that has accreted during the 15-plus minutes in icing conditions.

Figure 12 provides the calculated ice thickness as a function of distance along the airfoil, s. At this wing station the maximum ice thickness is approximately 0.175 inches and occurs aft of the leading edge on the upper surface with a second peak of 0.12 inches located aft of the leading edge on the lower surface. In this case the two peaks are indicative of the beginning of the formation of horns which are characteristic of clear or glaze ice. Again, the ice is thicker than at locations W01 and W02 since the airfoil is smaller and thinner making it a more efficient ice collector. The accreted ice significantly alters the leading edge of the airfoil which will result in a degradation in the aerodynamic performance of the airfoil as will be discussed later. As was the case with the ice shapes at wing stations W01 and W02 the ice does not accrete very far back on the upper surface and would be well within the coverage of the upper de-icing boots. A very thin layer of ice extends farther aft on the lower surface; however, its effect on the aerodynamics of the wing will be minimal.

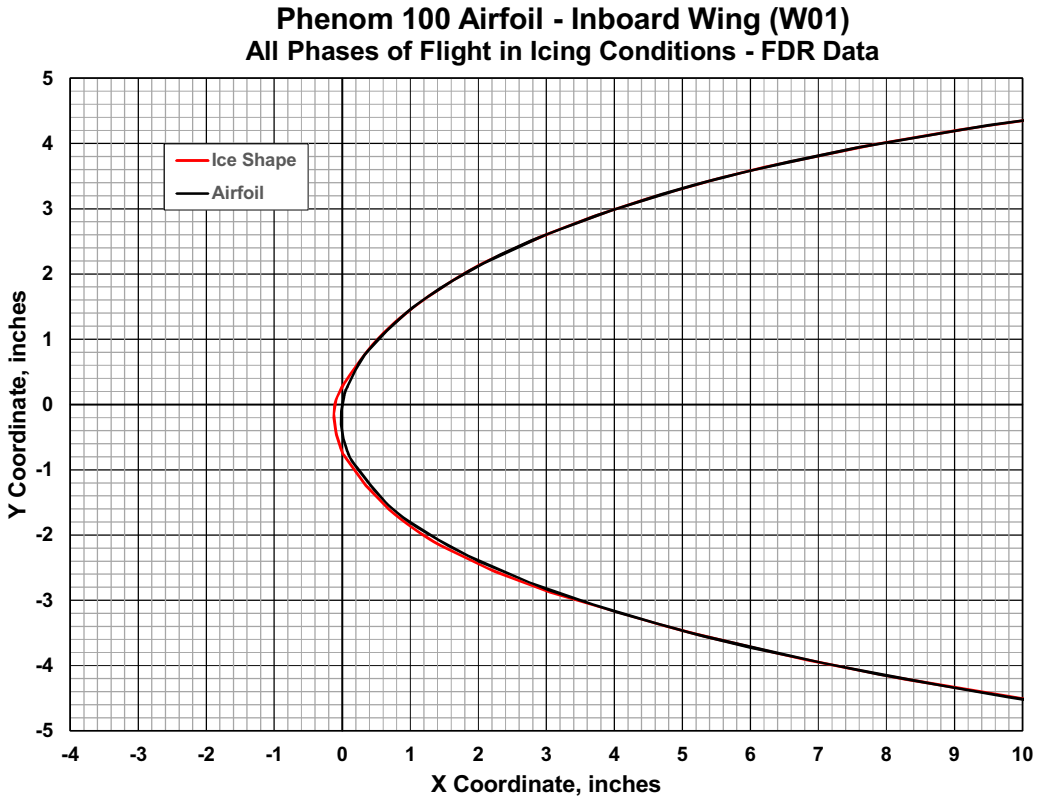

Figure 4. Airfoil and Ice Shape at Location W01 in the Icing Environment

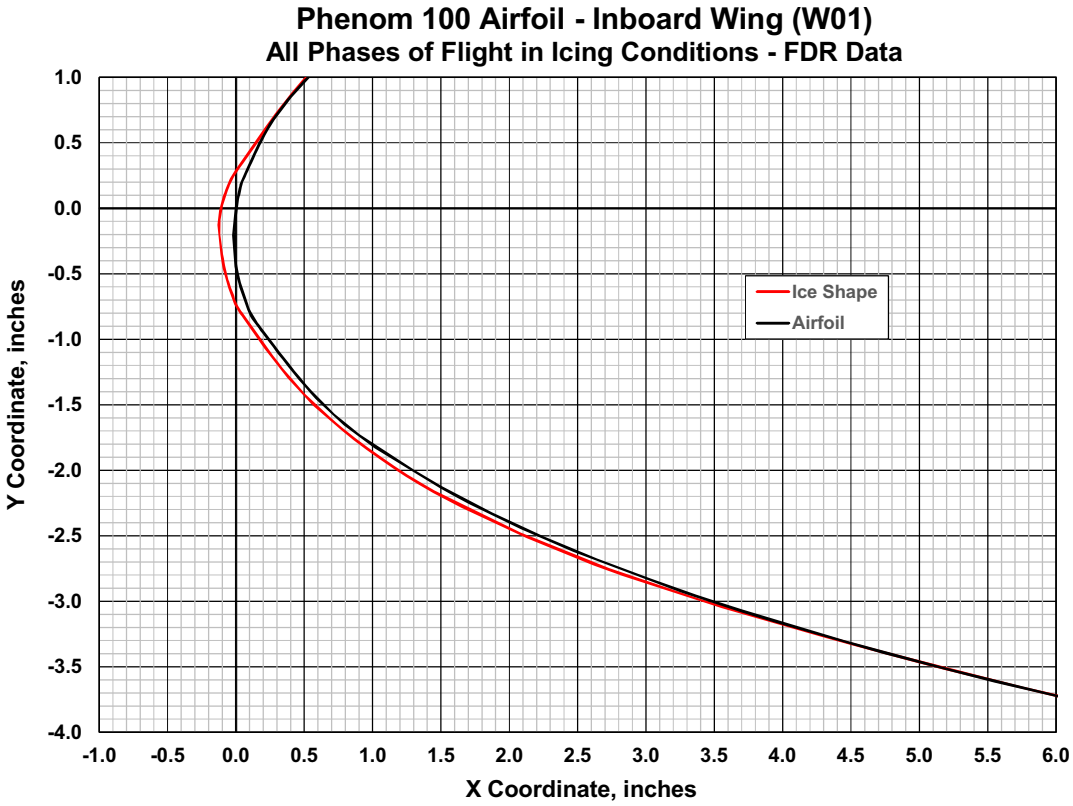

Figure 5. Airfoil and Ice Shape at Location W01 in the Icing Environment (Close-up)

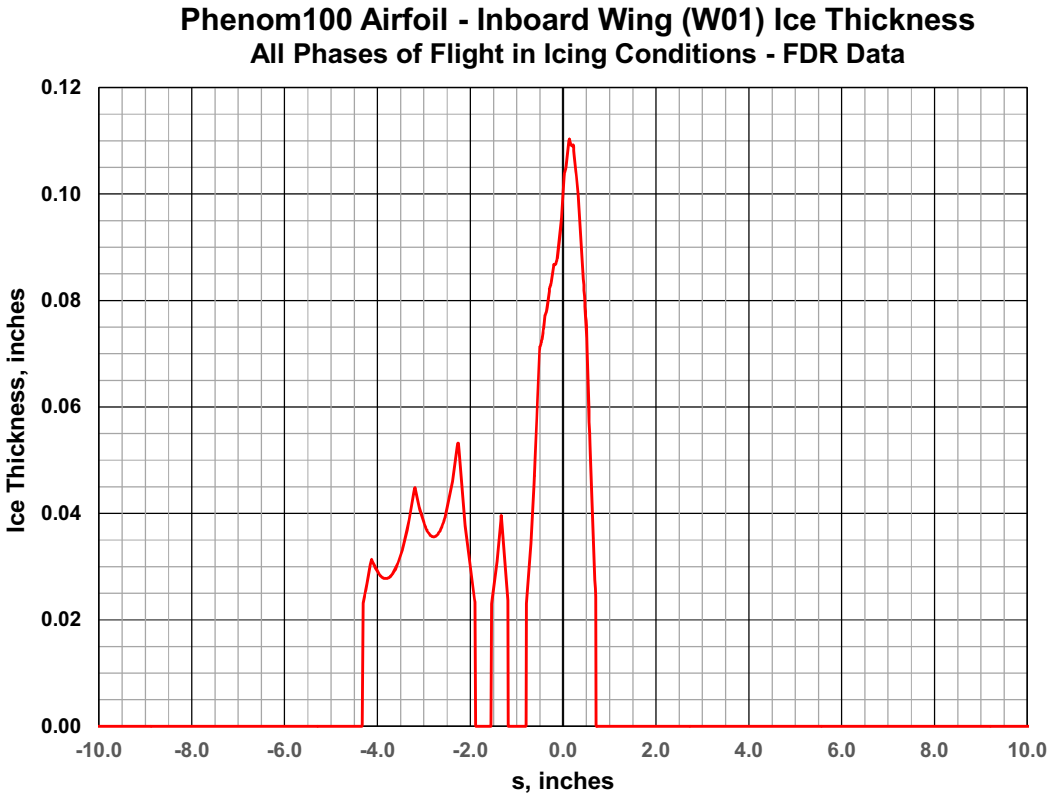

Figure 6. Ice Thickness as a Function of Distance Along the Surface of the W01 Airfoil, s

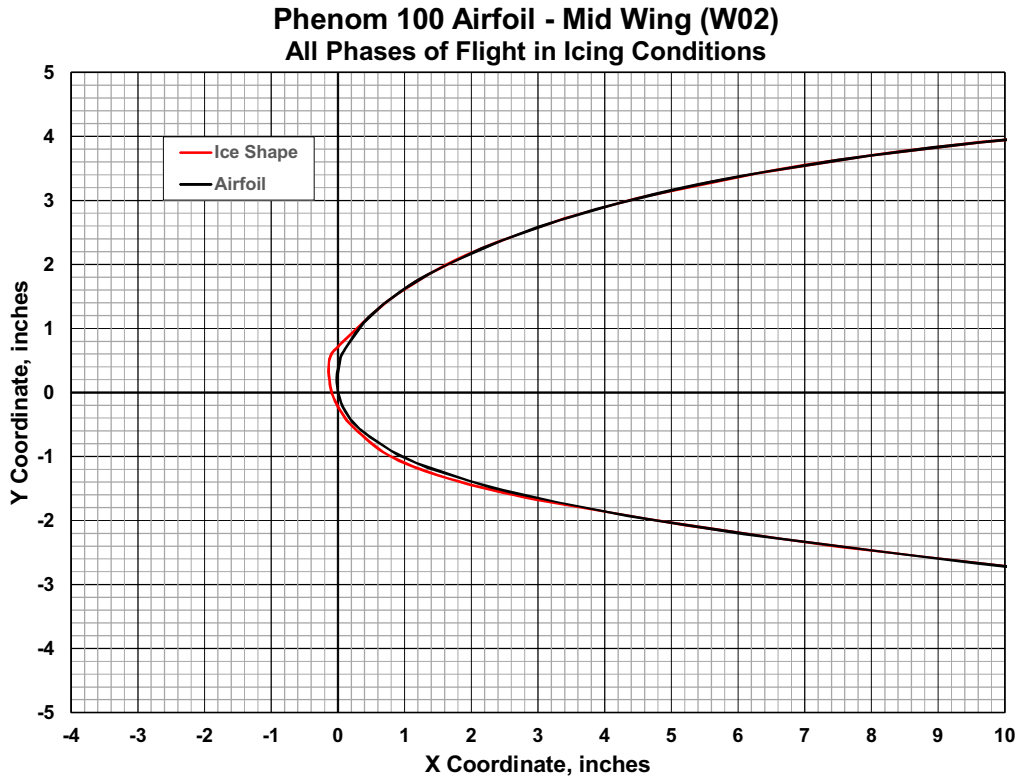

Figure 7. Airfoil and Ice Shape at Location W02 in the Icing Environment

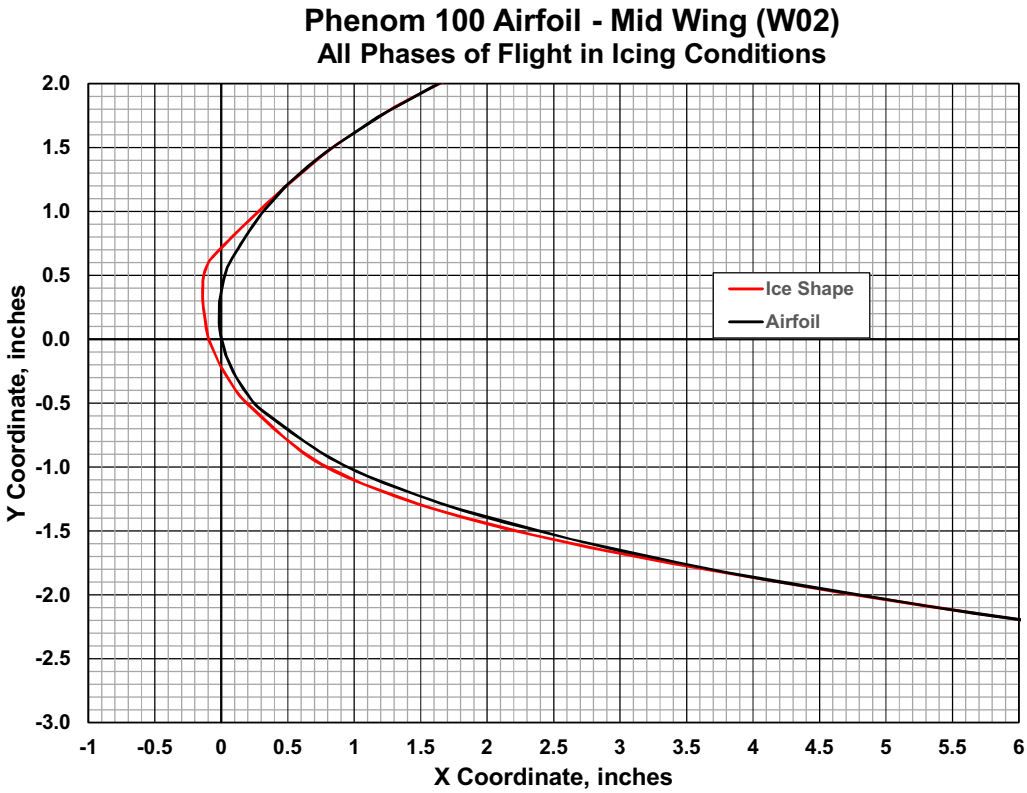

Figure 8. Airfoil and Ice Shape at Location W02 in the Icing Environment (Close-up)

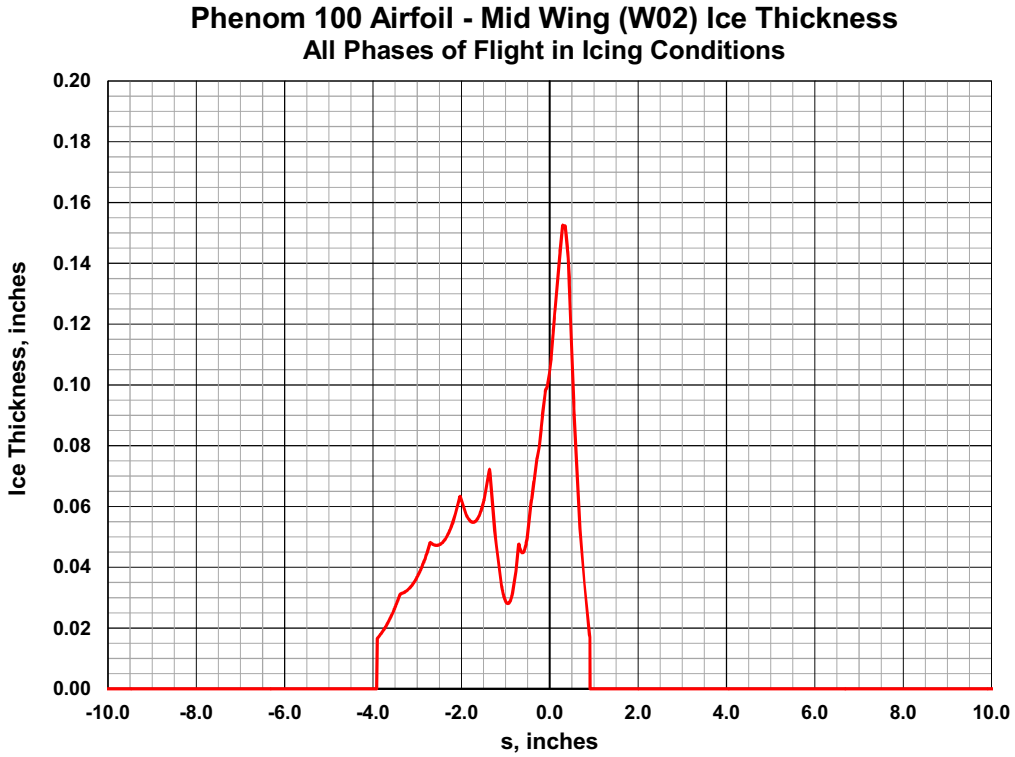

Figure 9. Ice Thickness as a Function of Distance Along the Surface of the W02 Airfoil, s

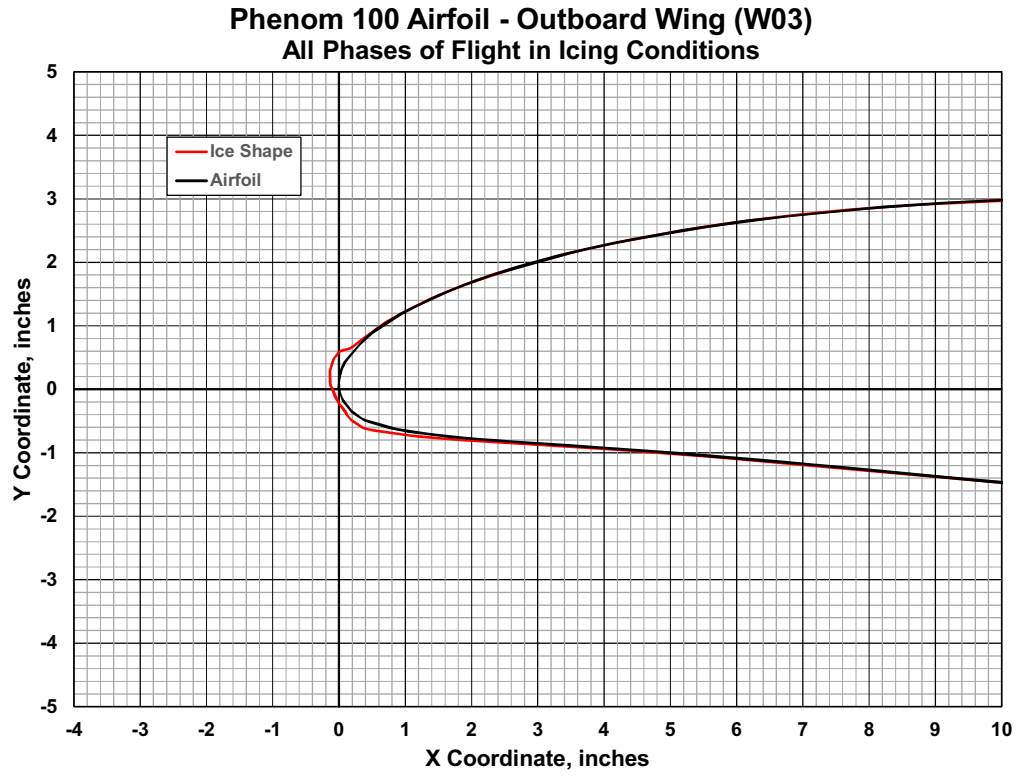

Figure 10. Airfoil and Ice Shape at Location W03 in the Icing Environment

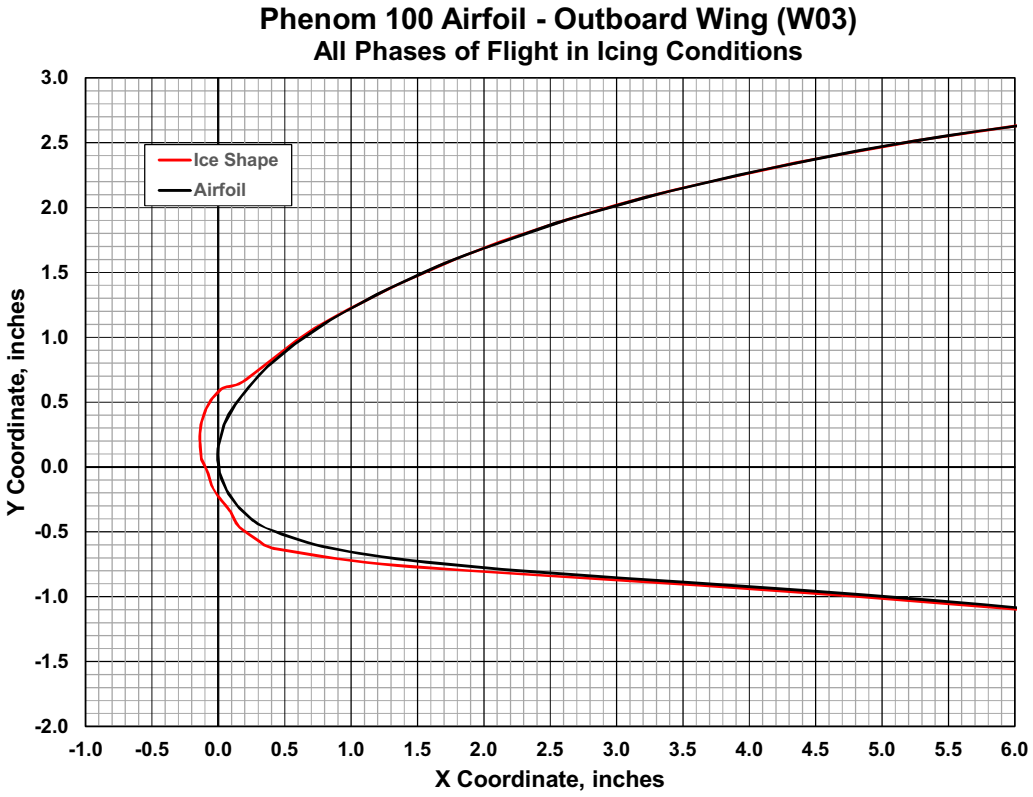

Figure 11. Airfoil and Ice Shape at Location W03 in the Icing Environment (Close-up)

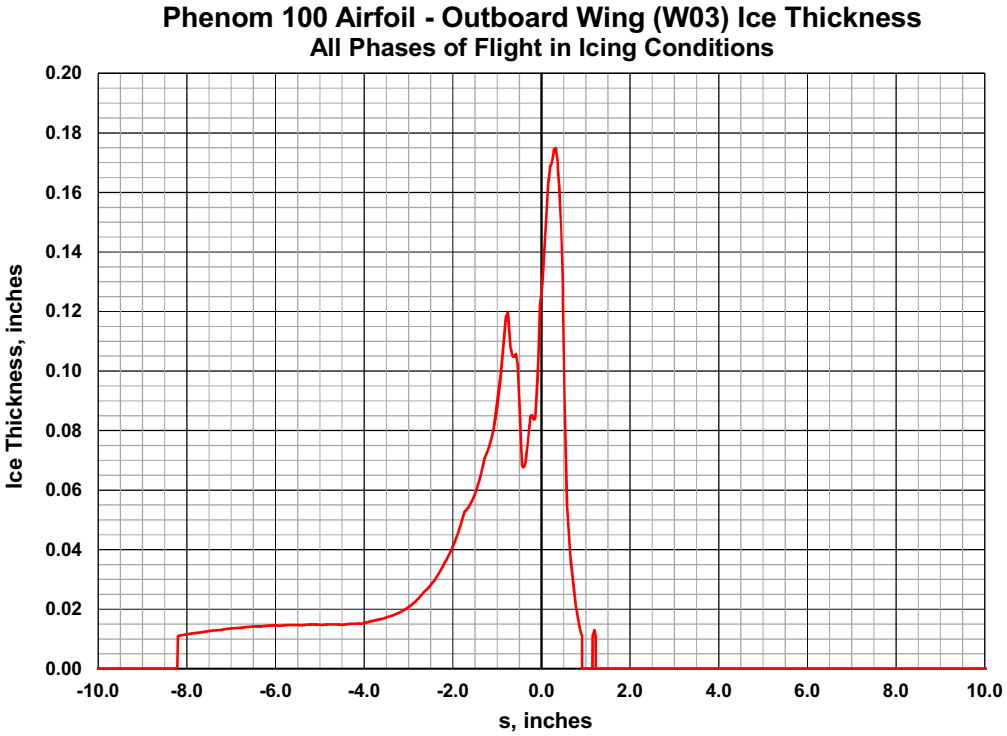

Figure 12. Ice Thickness as a Function of Distance Along the Surface of the W03 Airfoil, s

Horizontal Tail Cross section HT01 (Inboard Horizontal Tail Section) Results

The forward part of the horizontal tail airfoil section and ice shape at location HT01 is shown in Figure 13. A close-up of the forward part of the airfoil in Figure 14 better reveals the ice that has accreted during that the 15-plus minute icing encounter.

The calculated ice thickness as a function of distance along the airfoil, s, is shown in Figure 15. At this station the maximum ice thickness is approximately 0.34 inches and occurs very near the leading edge of the airfoil on the upper surface. As expected there is a larger amount of ice accretion on the horizontal tail than on the wing since it is smaller and thinner, and therefore, a more efficient ice collector. Recall that the maximum thickness of the ice on wing varied from 0.11 inches on the inboard section to slightly greater than 0.175 inches on the outboard section.

Horizontal Tail Cross Section HT02 (Mid-Span Horizontal Tail Section) Results

The horizontal tail airfoil and ice shape at location HT02 is shown in Figure 16. A closer view of the forward part of the airfoil in Figure 17 better reveals the dimensions of the ice that has accreted while operating in the icing conditions. In comparing this ice shape with that of HT01 there is more ice since it is a thinner, smaller airfoil with a higher collection efficiency.

The calculated ice thickness as a function of distance along the airfoil surface, s, is shown in Figure 18. At this station the maximum ice thickness is approximately 0.39 inches and occurs near the leading edge of the airfoil. The ice does not accumulate very far aft on the upper and lower surfaces of the airfoil and would be within the coverage of the pneumatic de-icing boots.

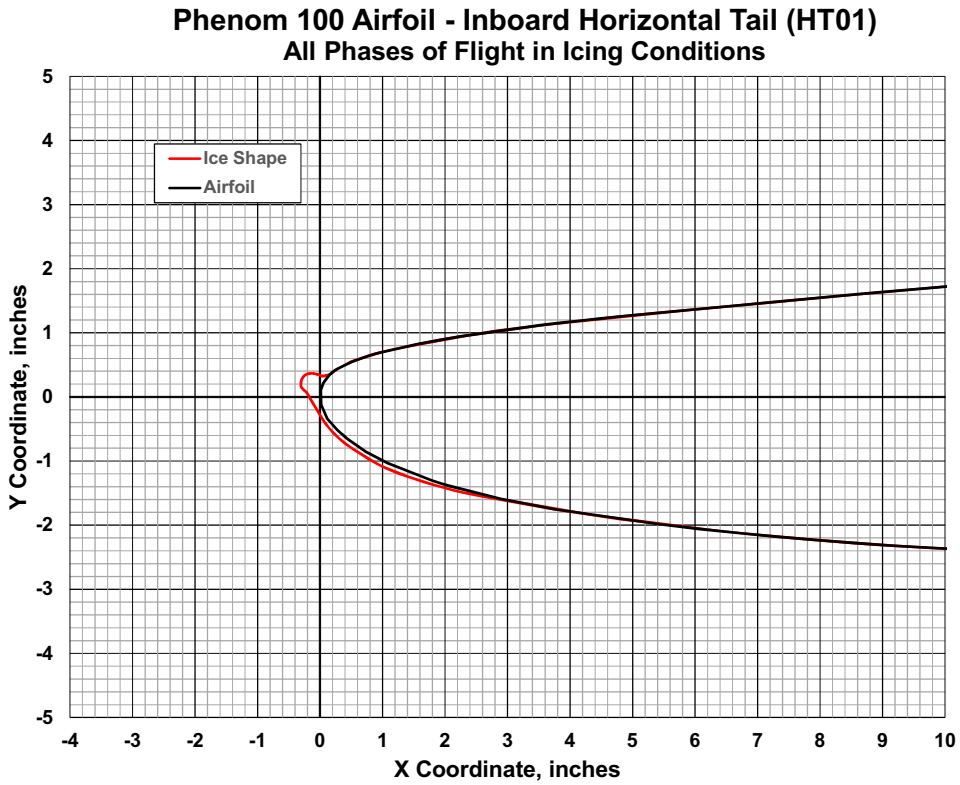

Figure 13. Airfoil and Ice Shape at Location HT01 in the Icing Environment

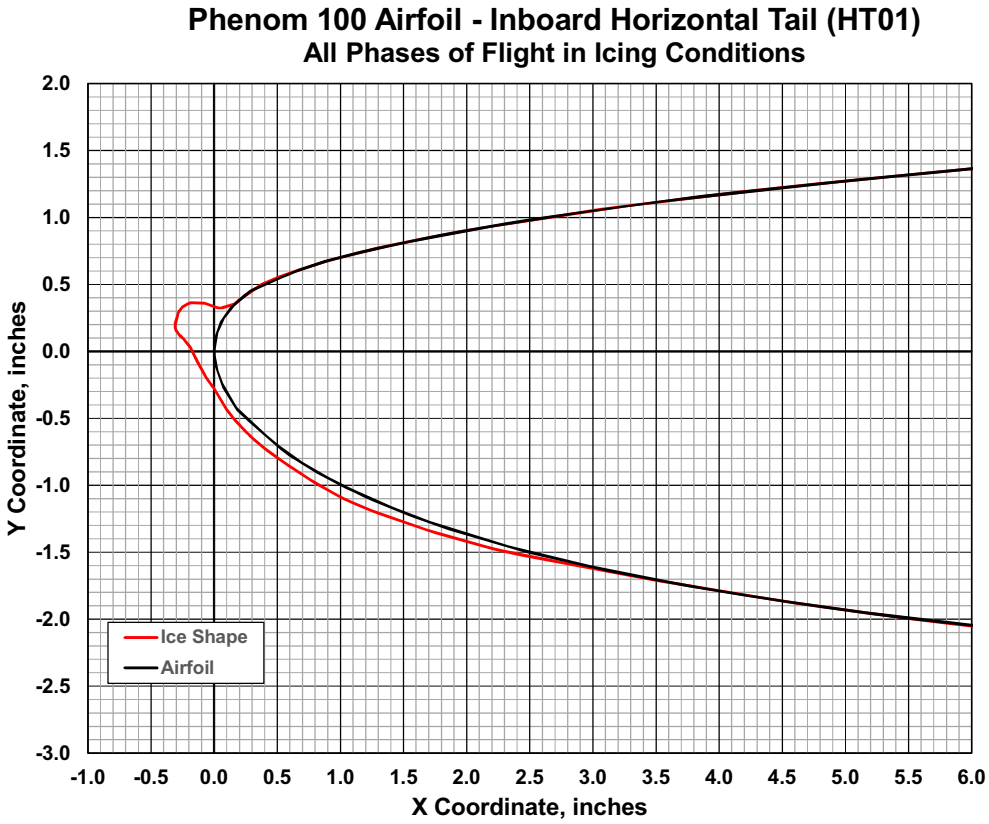

Figure 14. Airfoil and Ice Shape at Location HT01 in the Icing Environment (Close-up)

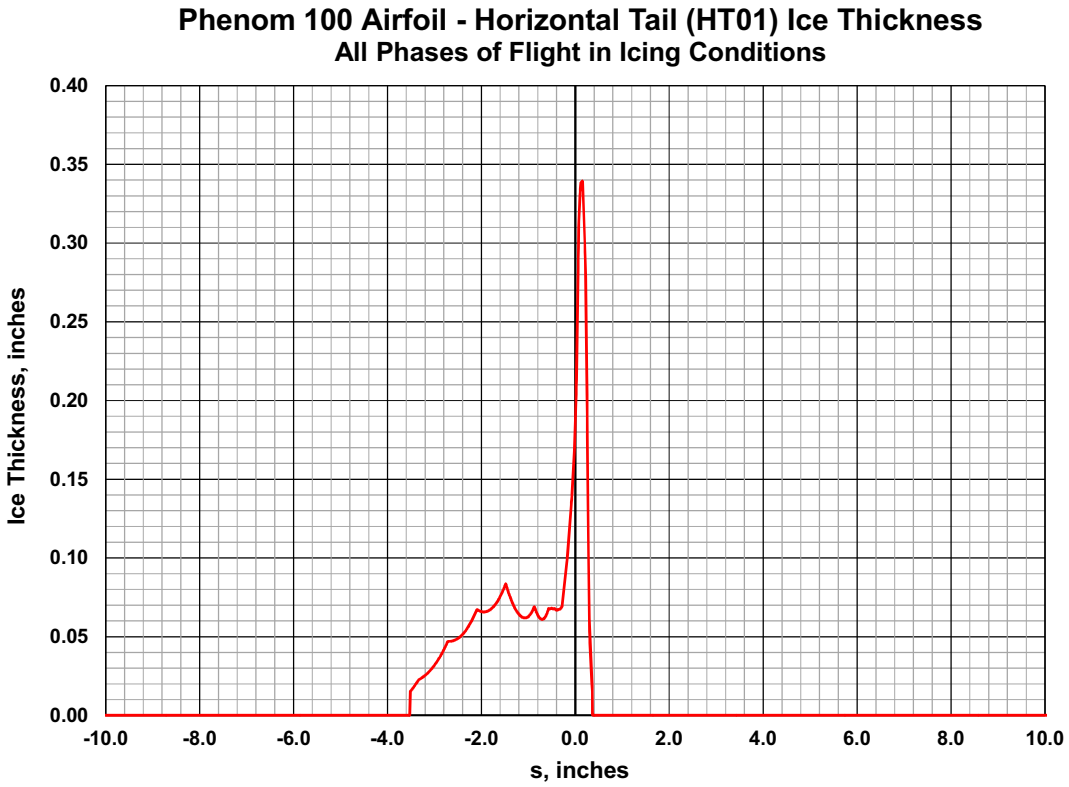

Figure 15. Ice Thickness as a Function of Distance Along the Surface of the HT01 Airfoil, s

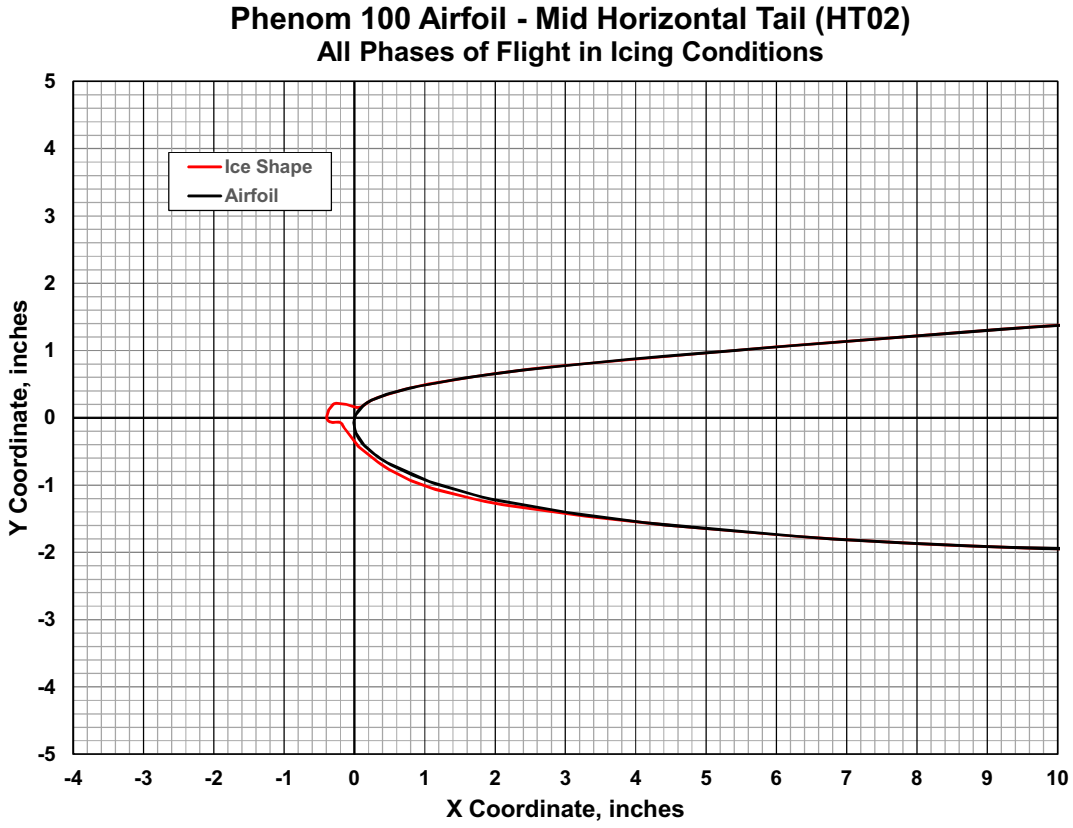

Figure 16. Airfoil and Ice Shape at Location HT02 in the Icing Environment

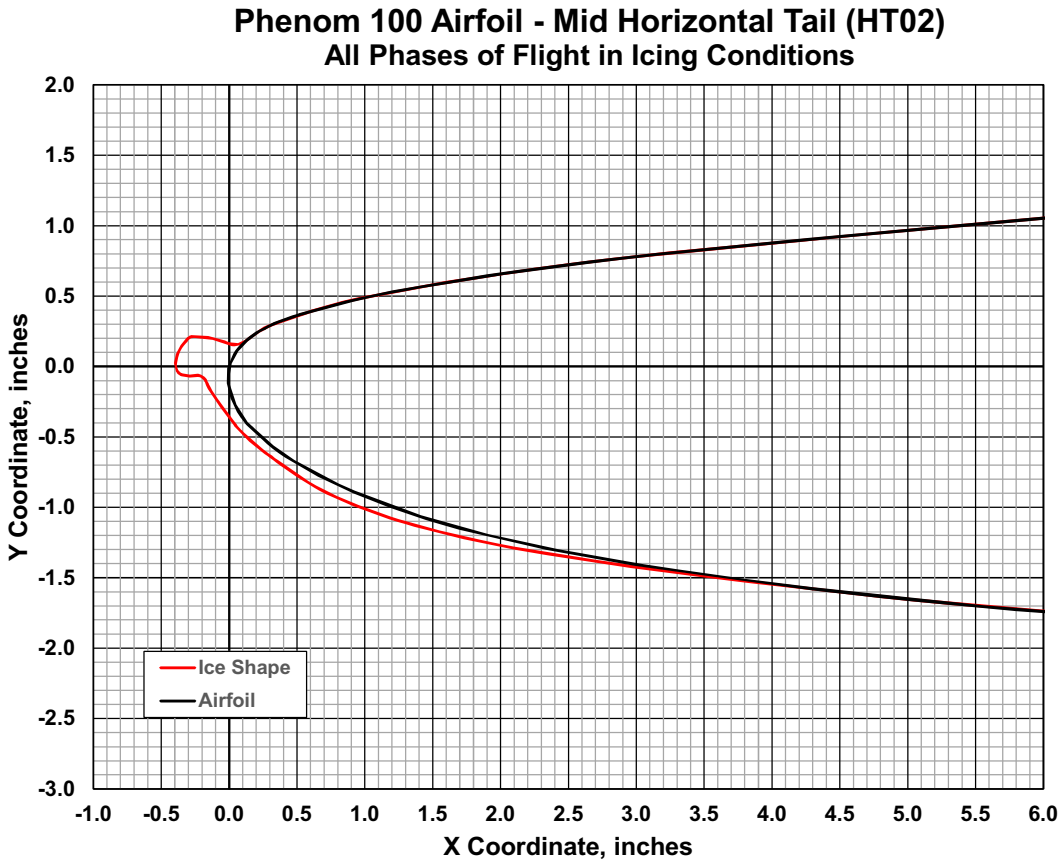

Figure 17. Airfoil and Ice Shape at Location HT02 in the Icing Environment (Close-up)

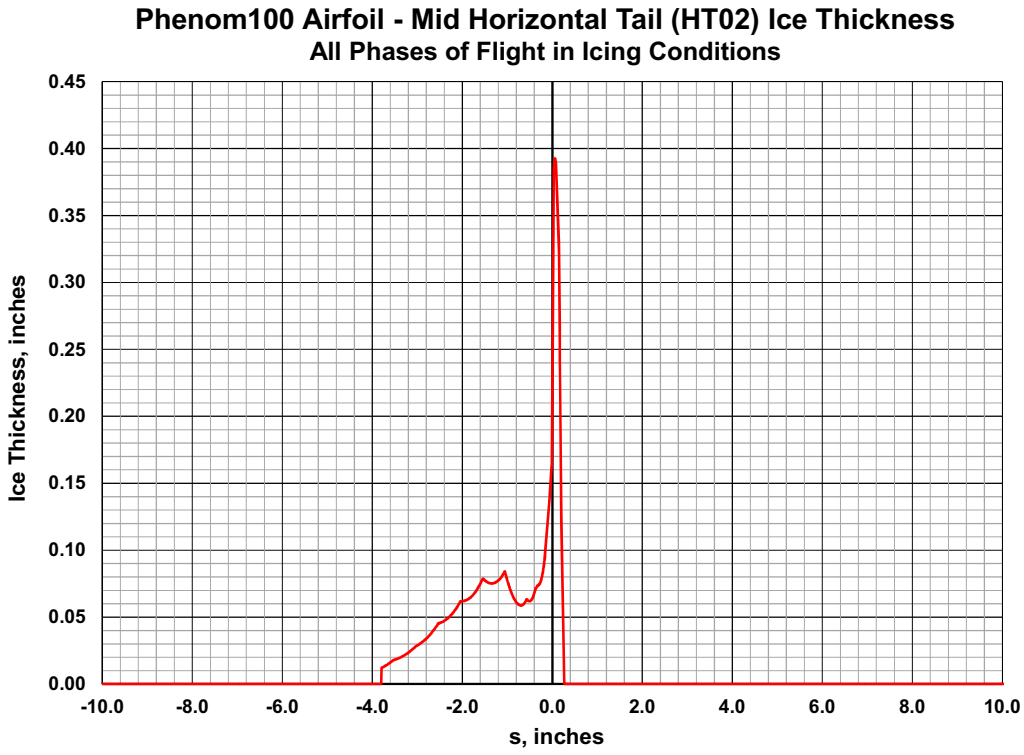

Figure 18. Ice Thickness as a Function of Distance Along the Surface of the HT02 Airfoil, s

Horizontal Tail Cross section HT03 (Outboard Horizontal Tail Section) Results

The forward part of the horizontal tail airfoil section and ice shape at location HT03 is shown below in Figure 19. Figure 20 provides a closer view of the leading edge of the airfoil and the ice accretion.

The calculated ice thickness as a function of distance along the airfoil surface, s, is shown in Figure 21. At this station the maximum ice thickness is approximately 0.21 inches slightly below the leading edge point with a second peak of near 0.19 inches slightly above the leading edge point. As was the case with the outboard section of the wing this exhibits the beginning of the formation of two ice horns which is indicative of clear ice. This ice does not conform to the leading edge of the airfoil and significantly changes the shape and aerodynamics of that part of the tail.

AERODYNAMIC EFFECTS ON CONTAMINATED AIRFOILS

The analysis examined the amount of ice accumulation on six cross-sectional cuts from the wing and the horizontal tail of the type that is on the Embraer 500 Phenom 100 aircraft. On the leading edge of the wing the ice thickness varied from a maximum thickness of 0.11 inches on the inboard section to greater than 0.15 inches on the mid-span section to approximately 0.175 inches on the outboard section. As the spanwise location increases, the ice shape begins to exhibit the beginning of upper and lower horns which is indicative of glaze or clear ice.

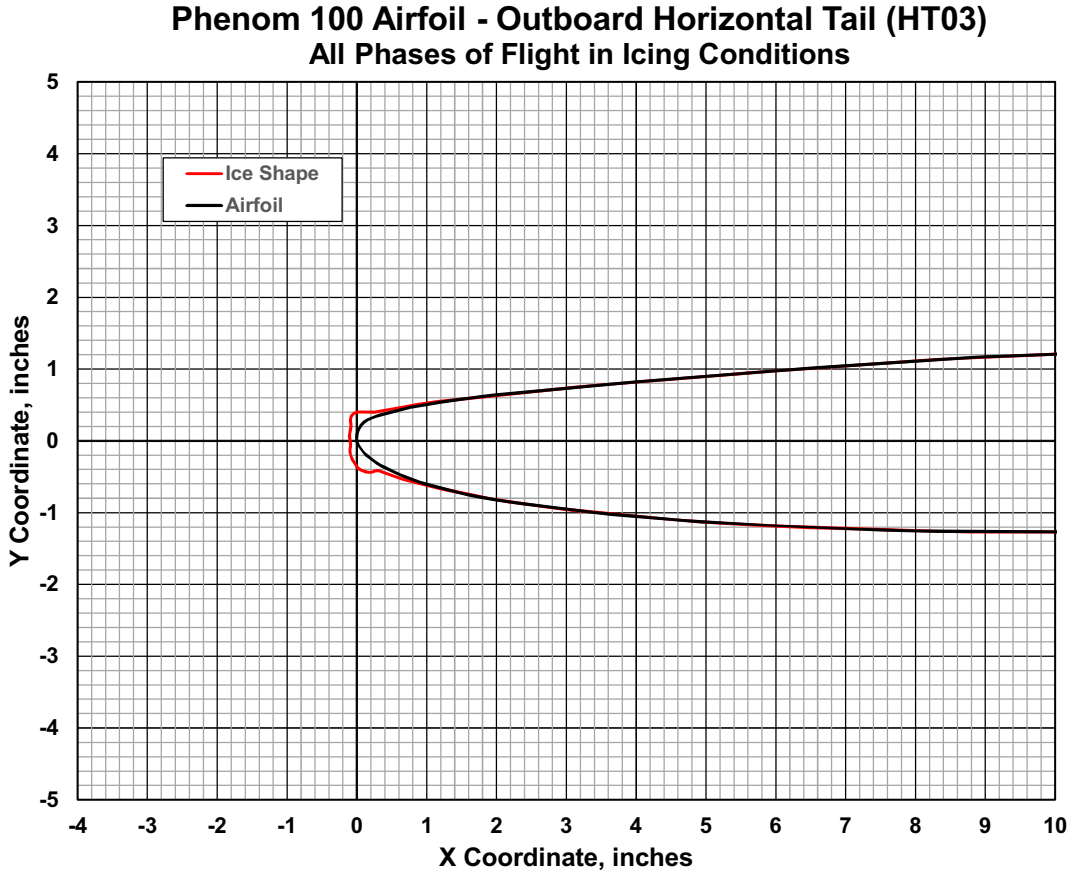

Figure 19. Airfoil and Ice Shape at Location HT03 in the Icing Environment

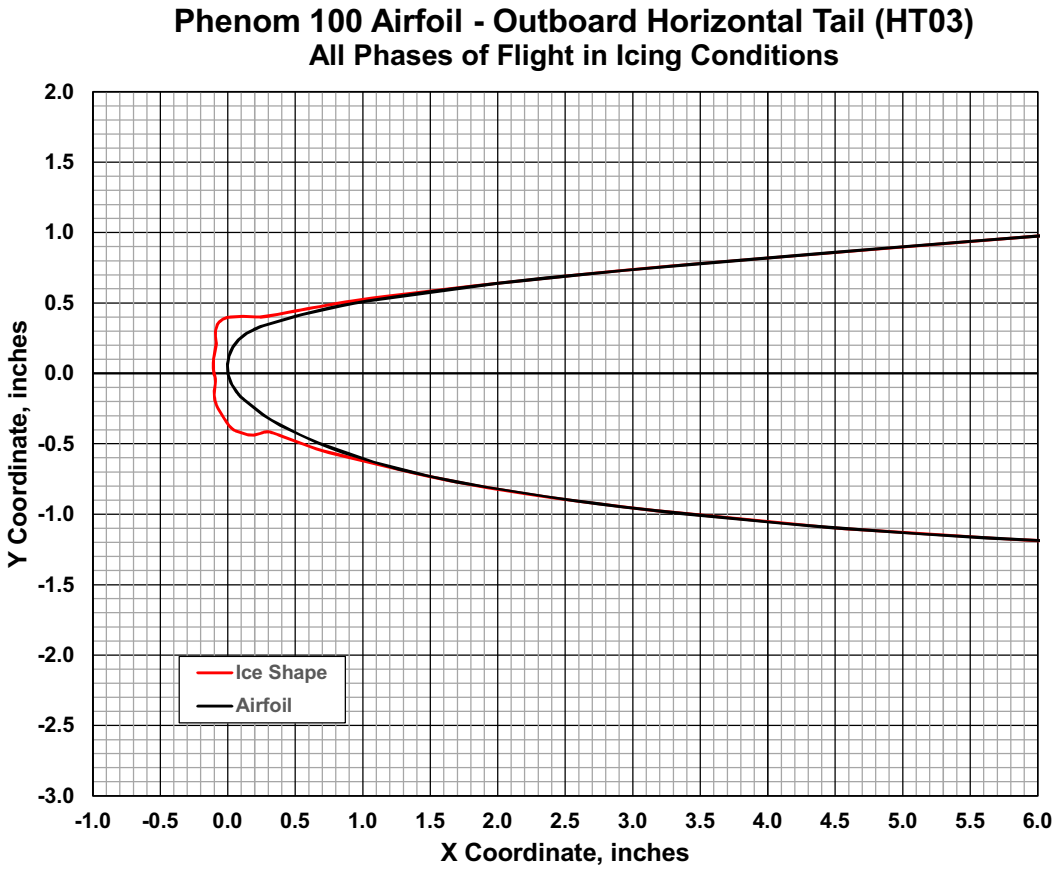

Figure 20. Airfoil and Ice Shape at Location HT03 in the Icing Environment (Close-up)

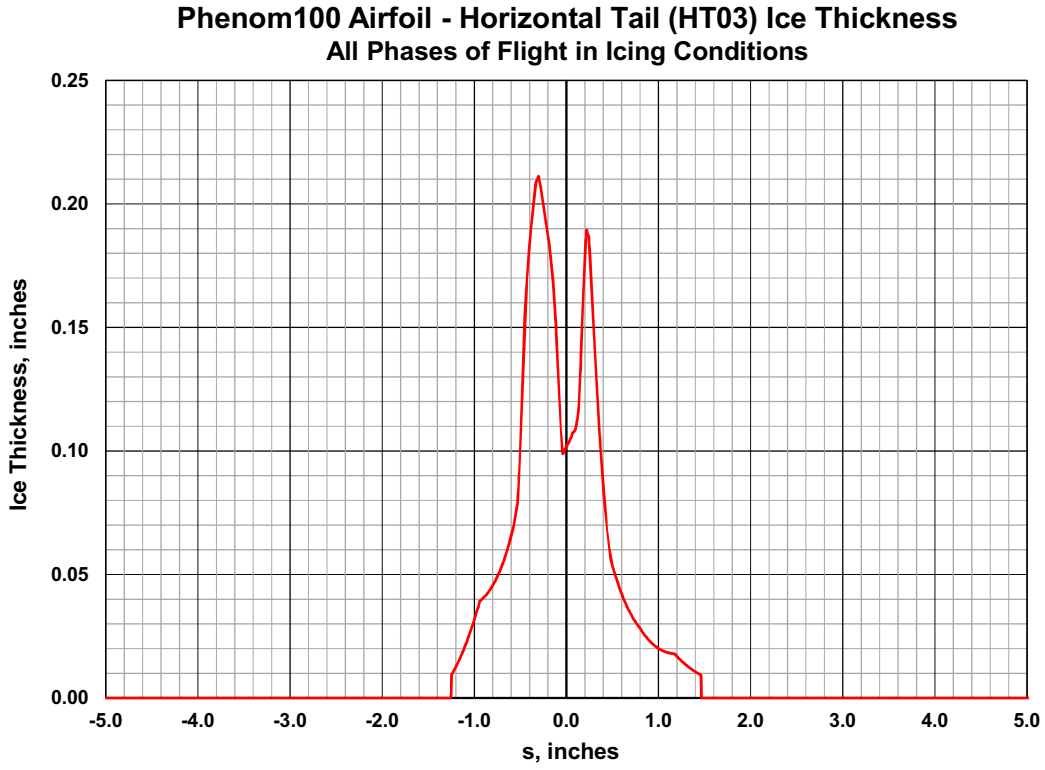

Figure 21. Ice Thickness as a Function of Distance Along the Surface of the HT03 Airfoil, s

The following discussion presents the aerodynamic effects on contaminated airfoils, considering typical airfoils, not those of Phenom 100 that were employed on the LEWICE study. Figure 22 shows a lift curve for a typical airfoil depicting the coefficient of lift plotted versus the angle of attack.[6] For a clean airfoil without roughness the maximum lift coefficient and stall angle of attack is identified on the plot with dashed red lines. For the same flow condition and the same airfoil type but with a standard roughness applied to a region around the leading edge of the surface, both the maximum lift coefficient and the angle of attack at which the airfoil stalls are reduced. It is very important to note that this reduction in maximum lift coefficient and reduction in stall angle attack occurs solely due to adding a standard surface roughness to the airfoil and not from the accretion of ice shapes on the airfoil.

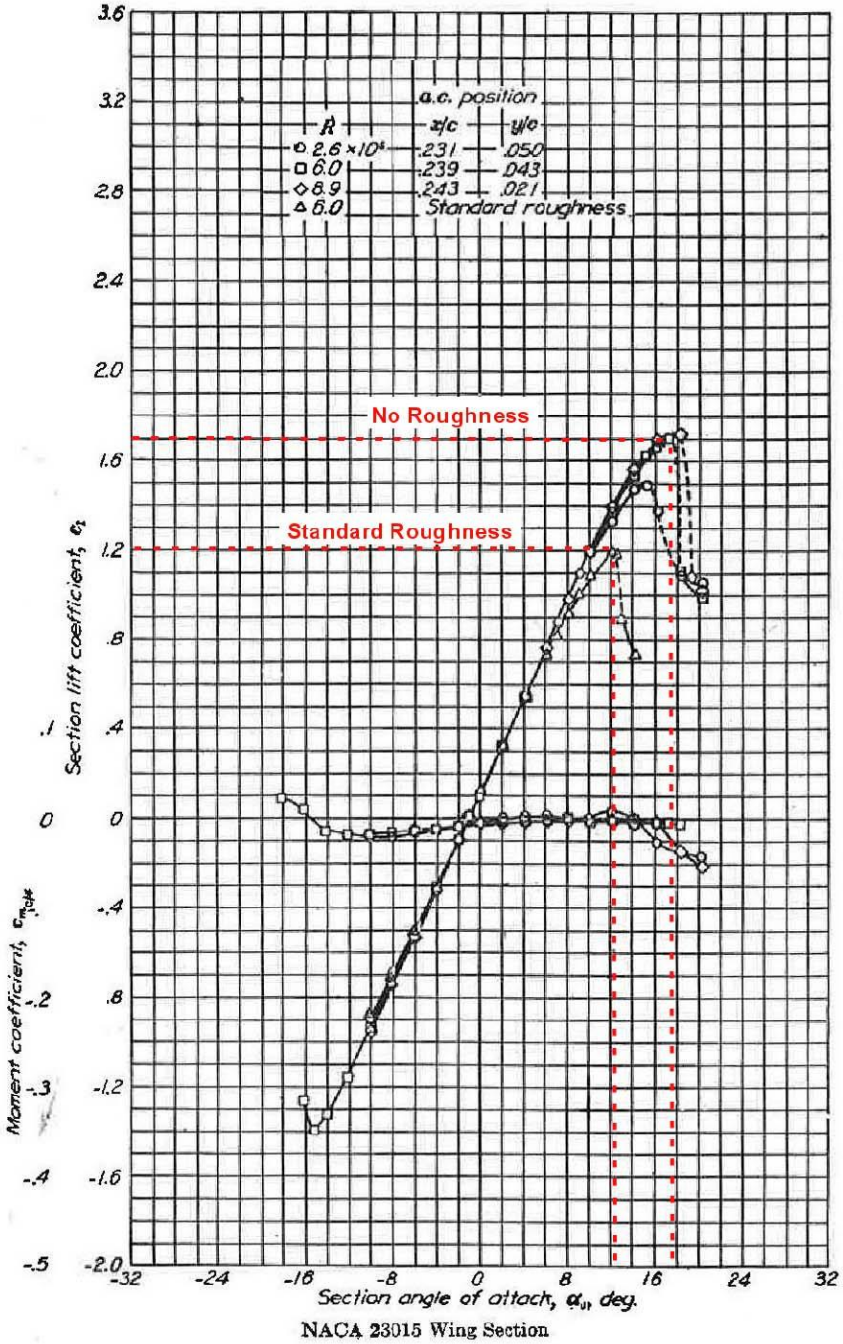

Figure 22. Lift Curve for Typical Wing Section (Airfoil)[6]

A typical effect of ice contamination on the lift curve for a wing (also unrelated to the Phenom 100 LEWICE analysis) is shown below in Figure 23.[7] As illustrated in Figure 22, this plot shows that even the introduction of some roughness on the leading edge of the wing results in a reduction of the maximum lift coefficient, C_{Lmax}, and decrease in the stall angle of attack. The reduction in C_{Lmax} and stall angle of attack becomes even greater with the introduction of ice shapes and is most severe when ice horns form.

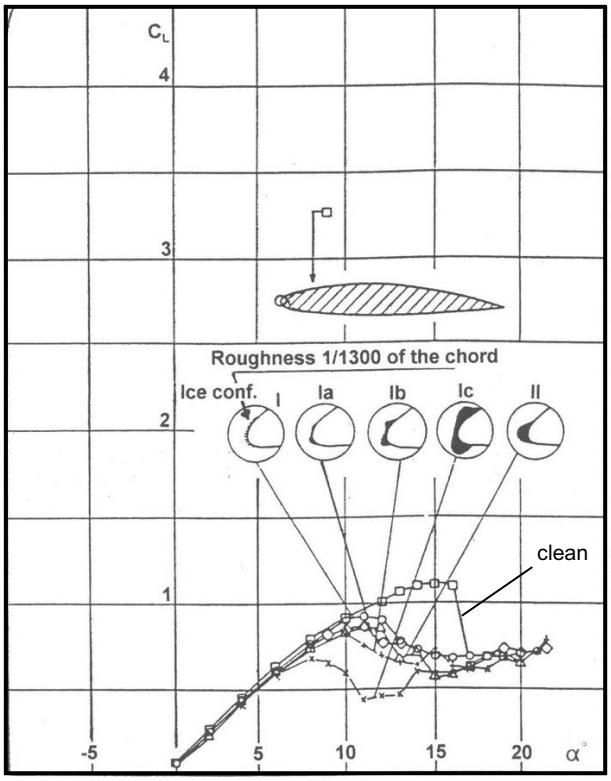

Figure 23. Effects of Ice Shapes on Lift Curve from Icing Tunnel[7]

The decrease in C_{Lmax} results in an increase in stall speed, V_{stall}, as shown in the equation

$$V_{stall} = \sqrt{\frac{2W}{\rho C_{L\max} S}}$$

where W is the aircraft weight, ρ is the air density, and S is planform area of the wing. Therefore, the formation of any ice will result in an increase in stall speed for the aircraft due to the decrease in the stall angle of attack and C_{Lmax}. This requires the aircraft to operate at a higher approach and landing airspeed to avoid a stall than would be appropriate for a non-contaminated aircraft. Additionally, the normal stall warning for an aircraft without contamination due to ice might be below the actual stall speed (stall angle of attack) of the contaminated aircraft providing no warning to the pilot. Therefore, it is critical to operate the aircraft's ice protection systems when in icing conditions to remove any ice that is accreted during the flight. The Airplane Flight Manual (AFM)[8] for the Phenom 100 states:

> Crew must activate the ice protection system when icing conditions exist or are anticipated as follows:
>
> If SAT (TAT inflight) is between 5°C and 10°C with visible moisture:
> ENG 1 & 2 Switches..... ON
> WINGSTAB Switch.....OFF
> WSHLD 1 & 2 Switches.....OFF
>
> At the first sign of ice formation or if SAT (TAT inflight) is below 5°C with visible moisture:
> WSHLD 1 & 2 Switches.....ON
> ENG 1 & 2 Switches..... ON
> WINGSTAB Switch.....ON

Note that the WINGSTAB Switch to ON refers to activating the pneumatic boots on the wing and horizontal stabilizer which must be performed by the crew at either the first sign of ice formation or if the static air temperature (SAT) or total air temperature (TAT) inflight is below 5°C with visible moisture (in clouds). In addition to the system removing the accreted ice on the wing and horizontal tail, activation of the ice protection system on the Phenom 100 results in the stall warning initiating at a lower angle of attack than normal. With the flaps and gear up the stall warning initiates at a vane angle of attack 5.5 degrees lower than it would without the ice protection system on[9]. With flaps and landing gear down the stall warning initiates at a vane angle of attack 11.5 degrees lower when the ice protection is on[9]. In the case of the accident flight, if the WINGSTAB switch had been on, the stall warning would have activated well before the aircraft reached stall alerting the pilot to reduce the angle of attack and keep the airspeed up.

In addition to the decrease in stall angle of attack and increase in stall speed, any asymmetric ice formation between the two wings can lead to one wing losing lift before the other one resulting in an unexpected roll and potential loss of control. This is especially true of an asymmetry on the outboard sections of the wing in front of the ailerons where the ice buildup is most severe as shown in the LEWICE results.

On the horizontal tail the ice thickness reached a maximum of 0.39 inches at the mid-span location and exhibited the beginning of two ice horns and a significant change in the shape of the leading edge at the outboard (HT03) section. As expected the ice of the horizontal tail is thicker than on the wing since it is a more efficient ice collector. The ice accretion on the horizontal tail will also reduce the effectiveness of the tail; however that does not appear to be the issue in this accident.

CONCLUSIONS

The analysis using the validated NASA LEWICE 3.2.2 icing code provides a good indication of the ice that would have accreted on the wings and horizontal tail of N100EQ during the 15-plus minutes the aircraft was operating in icing conditions.

There is no doubt that ice formed on the aircraft during the approach based on the meteorological and flight conditions. The CVDR indicated that the ice protection system was not used; therefore, any ice that accreted would have stayed on the aircraft during the approach. This accretion of this ice would have caused the aircraft to stall at a lower angle of attack and higher airspeed than normal. To precisely quantify this effect either a computational fluid dynamic analysis or experimental testing with the calculated ice shapes is required. Such an analysis was not a part of this LEWICE study.

Had the ice protection system been used during the icing encounter, several major benefits would have helped to minimize the effects of icing on N100EQ. First, the cycling of the pneumatic boots would have removed much of the accreted ice from the leading edges of the wing and the horizontal tail greatly reducing or eliminating the undesirable aerodynamic effects that result in premature stall. Second, the use of the ice protection system would have decreased the angle of attack and increased the airspeed when the stall warning initiated providing an earlier warning to the pilot. This earlier warning would have occurred while the aircraft was at an airspeed above the increased stall airspeed due to ice contamination.

REFERENCES

1. **Data and Drawings supplied from Embraer S.A.,** 2015.

2. **Users Manual for the NASA Glenn Ice Accretion Code LEWICE (Version 3.2.2)**, NASA Contractor Report, NASA Glenn Research Center, Ohio, 2004.

3. **Validation Report for LEWICE 2.0**, NASA CR 208690, January 1999.

4. **http://www.americankestrelco.com**

5. **Meteorological and Icing Data supplied by Dr. Wayne Sand,** 2015.

6. Abbott, I. H. and von Doenhoff, A. E., **Theory of Wing Sections: Including a Summary of Airfoil Data**, Dover Books, 1959.

7. **Aircraft Icing: Meteorology, Protective Systems, Instrumentation, and Certification Course,** University of Kansas Continuing Education Program, University of Kansas, Lawrence, KS.

8. **Phenom 100 FAA Airplane Flight Manual**, Embraer, S.A., December 2008.

9. **NTSB Aircraft Performance Study**, Timothy Burtch, 2016.